IEEE Access
Multidisciplinary | Rapid Review | Open Access Journal

Received January 14, 2022, accepted February 6, 2022, date of publication February 10, 2022, date of current version February 23, 2022.

*Digital Object Identifier 10.1109/ACCESS.2022.3151027*

# A Forward Scattering Model in Two-Dimensional Half-Space for Scatterers' Size Estimation Using Linear Inversion

**SOUMYAKANTI MAITI[1], (Graduate Student Member, IEEE), AMITABHA BHATTACHARYA[2], (Senior Member, IEEE), AND KAUSHIK DEY[3]**

[1]Advanced Technology Development Center, Indian Institute of Technology Kharagpur, Kharagpur, West Bengal 721302, India
[2]Department of Electronics and Electrical Communication Engineering, Indian Institute of Technology Kharagpur, Kharagpur, West Bengal 721302, India
[3]Department of Mining Engineering, Indian Institute of Technology Kharagpur, Kharagpur, West Bengal 721302, India

Corresponding author: Soumyakanti Maiti (ec.skmaiti@gmail.com)

**ABSTRACT** Analytic expressions of scattered electric fields for different categories of cylindrical targets buried in the half-space have been developed. In all the cases, investigation domains have been considered two-dimensional and are infinitely long in the remaining dimension. The investigation domains have been excited by the fields generated by a z-directed line source of constant amplitude, operating in the microwave frequencies. The usefulness and validity of these scattering models have been examined by inversion of the scattered electric field generated by the same. The inversion is based on the fact that the scattered field is mapped by a linear operator containing the induced current density and Green's function of the investigation domain. On application of the incident field, the presence of a discontinuity in half-space induces the current density. By using the information retrieved from the reconstruction of current density by inversion and analytical expressions of the scattered electric field, information about the diameter and the type of the scatterer have been obtained. In addition, the performance of the linear sampling method for shape reconstruction of the scatterer in half-space is also explored.

**INDEX TERMS** Current density, green's function, half-space, inversion, microwave, scattered fields, scatterer.

## I. INTRODUCTION

The penetration capability of the microwave signal through the optically opaque areas encourages the researchers to explore its capability of detecting targets of interest in the hidden area. Inversion of the scattered electric field at microwave frequencies, measured on the limited number of spaces, known as microwave imaging, helps to recover the parameters characterizing the object of interest [1]. An alternative approach to microwave imaging is microwave detection, used by Ground Penetrating Radars (GPR) or through-the-wall radars to detect the existence of targets having constitutive parameters different from the background [2]. An application of microwave signals in detecting human beings is available in [3]. In general, microwave inverse problems are non-linear. However, in certain cases, the inversion can be linearized [4]. Linear inversion, a qualitative method, helps to infer only the position and approximate geometrical shape of the target [4]. On the other hand, the non-linear inversion, also known as the quantitative method, can provide the exact distribution of the electrical parameters of the target of interest [5], [6]. Based on the mathematical models of the cost function, the non-linear inversion can be categorized into two classes [7]. The first one of its classes is the Newton-iterative type [8], [9], and the remaining one is known as the Contrast Source Inversion (CSI) [10], [11]. A study on microwave inversion using the combination of the Newton-iterative method and CSI is also reported in [12]. The linearized inversion, being simple, is popularly used. The most commonly used linearized inversion methods are the Born Approximation (BA) for detecting the dielectric target and the Kirchoff's Approximation (KA) for reconstructing the Perfectly Electrical Conductors (PEC). Application of these methods in half-space geometry is reported in [4], [13]–[16]. In some iterative methods, the contrast function is determined and updated by using a linearized inversion in

The associate editor coordinating the review of this manuscript and approving it for publication was Karu Esselle.

each iteration [17], [18]. An application of linearized CSI for imaging a three-dimensional half-space is available in [19]. Linear Sampling Method (LSM) is also another popular qualitative inversion method used to determine the shape of the unknown scatterer [20]–[23]. LSM is introduced to detect the non-penetrable scatterers like PEC based on the far-field scattering data [24]. However, it has been extended for detecting the penetrable scatterers and also in near-field cases [21], [22]. The scope of the LSM in the half-space investigation scenario is also studied and reported in [25]–[27]. Due to the inherent nature of the half-space geometry, it is quite natural that the object buried in half-space does not get fully illuminated by the fields from all directions. In [28], an attempt is made to predict the electric fields in the shadow region created by the targets in the investigation domain, and after that, the shape of the target is retrieved considering 3-D geometry. Depending on the occurrence of the observation scenario and the amount of information to be recovered, one needs to adopt different kinds of imaging configuration [29], [30]. The effective electrical parameters and the geometrical information of the targets are inferred in [31], [32] without considering the iterative methods. Another method, known as Orthogonality Sampling Method (OSM), similar to the LSM, is also applied to determine the shape of the anomalous target both for the far-field and near-field application [33]–[35]. Apart from this, Factorization Method (FM), Multiple Signal Classification (MUSIC), KA based shape reconstruction strategies, and many more can also be helpful in estimating the shape of the scatterer [36]–[39].

### A. RESEARCH ISSUE

In the case of GPR imaging, the geometry is always of half-space type. However, in the case of through-wall imaging, the half-space becomes a three-layered medium (air-wall-air). Based on the previous studies, the authors have observed that due to the limitation of illumination, LSM and other shape reconstruction methods become ineffective to reconstruct the shape of the target buried in half-space, thereby leading to localization only. Linearized inversion schemes based on BA and KA are comparatively simple and provide a reasonably acceptable result for locating the target in the half-space. Notably, the obtained results become more accurate if the proper linearization method (BA for dielectric reconstruction and KA for PEC) is chosen beforehand. Although, making the appropriate choice for detecting the unknown scatterer is difficult. These mentioned issues motivated the authors to explore the qualitative imaging methods and the analytical bases of the scattering models influencing them.

### B. AUTHORS' CONTRIBUTION

Based on the prevailing issues and getting inspired by [31], [32], the authors have emphasized the necessity of developing the forward scattering models for the specific scattering objects buried in the half-space. The capability of the inversion methods in extracting useful information can be improved by using the appropriate model of the scattered electric field. Thus, following are the contributions from the authors that make the article novel and unique:

- development of the analytical expressions for the scattered electric fields that are measured on the half-space boundary for a single PEC, a single dielectric, and two PEC cylindrical scatterers separately.
- study on the inversion methods in identifying the scattering objects in half-space, and also to prove the validity of the developed analytical expressions.
- proposition of a technique for retrieving the radius and type of the cylindrical target buried in two-dimensional half-space using the qualitative inversion and the mathematical models of the scattered electric field.

## II. ANALYTICAL EXPRESSIONS FOR THE FORWARD SCATTERING

In this section, the analytical expressions for the scattered electric fields are derived. In all the cases, the scattered electric fields have been measured on the half-space boundary. The primary purpose of deriving these analytical expressions in all such cases is to extend the capability of the linear inversion schemes to determine the exact size of the scattering object present in the half-space. Also, the developed models will help to avoid the dependency on the full-wave solvers. In all the cases, the geometry has been assumed to be located at the constant$-z$ plane. Also, the same has been assumed to be invariant along the $z-$direction. Different kinds of targets like a single dielectric cylinder, single PEC cylinder, and two PEC cylinders have been assumed to be buried in the lower half-space, and they generate the scattered fields on the application of the fields incident to the investigation domain. In the beginning, we will start with the generic forward scattering scenario. Figure 1 can be considered as a generic half-space investigation domain for the forward and the inverse scattering.

The upper half-space ($y < 0$) represents the air. The lower half-space ($y > 0$) represents the non-magnetic soil with generic relative permittivity $\epsilon_b$. It is worth noting that the term ''soil'' throughout the article can also be interpreted as a homogeneous non-magnetic medium with relative permittivity other than air. In general, $\epsilon_b$ can be a complex quantity, representing a lossy one. An arbitrarily shaped target $\Sigma$, having a two-dimensional cross-section with relative permittivity $\epsilon_r(x, y) \neq \epsilon_b$, has been assumed to be buried in the soil. The boundary of the target has been represented as $\partial\Sigma$ in Figure 1. The parameters $\underline{r}$ and $\underline{r}'$, respectively, represent the position vectors corresponding to $(x, y)$ and $(x', y')$. In Figure 1, the quantities $\mathcal{D}$ and $\mathcal{M}$, respectively, represent the investigation domain and the measurement line. The source points $(x_s, 0)$ and the observation points $(x_o, 0)$ are contained in $\mathcal{M}$. For the rest of the calculations, let us represent the incident electric field, scattered electric field, incident magnetic field and the scattered magnetic field, respectively, by $E_{inc}$, $E_{scat}$, $H_{inc}$, and $H_{scat}$. The total electric field $E_{tot}$ is the algebraic sum of the incident and the scattered electric fields. Similarly, the total

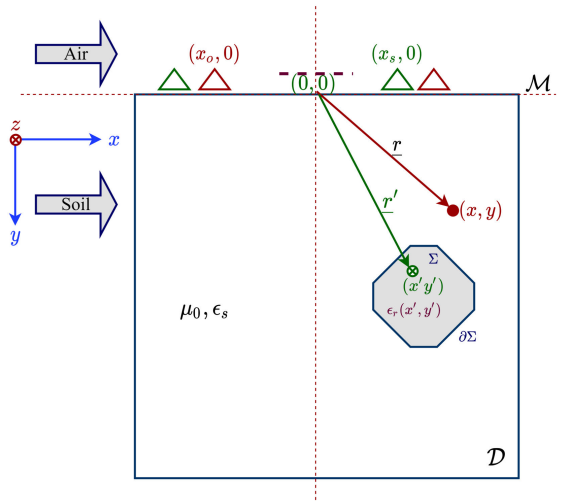


**FIGURE 1.** The generic investigation domain of half-space forward and inverse scattering.

magnetic field, $H_{tot}$ can be represented as the algebraic sum of the incident and the scattered magnetic fields. By solving Maxwell's equations for the total and incident fields, we get

$$\nabla^2 E_{scat}(\underline{r}) + k_b^2 E_{scat}(\underline{r}) = j\omega\mu_0 J_{eq}(\underline{r}'); \quad \underline{r} \notin \Sigma, \underline{r}' \in \Sigma. \tag{1}$$

The quantity $k_b = \omega\sqrt{\mu_0\epsilon_0\epsilon_s}$ and $J_{eq}(\underline{r}') = j\omega\epsilon_0[\epsilon_r - \epsilon_s]E_{tot}$ in chronology represent the wavenumber of the background medium and the current density induced due to the presence of the discontinuity of the relative permittivity. Equation (1) has a generic solution, and it is given as

$$E_{scat}(\underline{r}) = -j\omega\mu_0 \int_{\Sigma} J_{eq}(\underline{r}')G(\underline{r}, \underline{r}')d\underline{r}'; \quad \underline{r} \in \mathcal{D}. \tag{2}$$

The quantity $G(\underline{r}, \underline{r}')$ in (2) represents the fundamental solution of Helmholtz's equation in the homogeneous unbounded medium, and it is given as [40]

$$G(\underline{r}, \underline{r}') = -\frac{j}{4}H_0^{(2)}(k_b|\underline{r} - \underline{r}'|). \tag{3}$$

Thus, using (3) the generic solution provided in (2) can be derived for the half-space geometry. So,

$$E_{tot}(\underline{r}) = \begin{cases} E_{inc}(\underline{r}) + k_b^2 \int\limits_{\mathcal{D}} \left[\dfrac{\epsilon_r(\underline{r}') - \epsilon_s}{\epsilon_s}\right] G_{21}(\underline{r}, \underline{r}')E_{tot}(\underline{r}')d\underline{r}'; \\ \quad \underline{r} \in \mathcal{M} \\ E_{inc}(\underline{r}) + k_b^2 \int\limits_{\mathcal{D}} \left[\dfrac{\epsilon_r(\underline{r}') - \epsilon_s}{\epsilon_s}\right] G_{22}(\underline{r}, \underline{r}')E_{tot}(\underline{r}')d\underline{r}'; \\ \quad \underline{r} \in \mathcal{D}. \end{cases} \tag{4}$$

It is worth noting that the Green's functions, $G_{21}(\underline{r}, \underline{r}')$ (when observation is made at upper half-space and the scatterer is in the lower half-space) and $G_{22}(\underline{r}, \underline{r}')$ (when both the observation point and scatterer are lying in the lower half-space), used in (2) are the modified versions of (3). Modifications have been done to incorporate the reflection and the transmission at the air-soil boundary. The analytical expression for such kind of Green's function is well-established in literature [40].

### A. INCIDENT ELECTRIC FIELD IN HALF-SPACE

A point in a two-dimensional half-space effectively represents a line in the three-dimensional half-space. Therefore, a point source in the two-dimensional half-space effectively represents an infinite line source ($z-$directed with reference to Figure 1) in a three-dimensional half-space. Referring to [41], the electric field generated from an infinite line source with magnitude $I_0$, located at $(x_s, y_s)$ in the two-dimensional homogeneous medium containing the source, can be written as

$$E(\underline{r})_z = -\frac{I_0 k^2}{4\omega\epsilon}H_0^{(2)}(k|\underline{r} - \underline{r}_s|). \tag{5}$$

Here, $\underline{r}_s = x_s\hat{a}_x + y_s\hat{a}_y$ and $\underline{r} = x\hat{a}_x + y\hat{a}_y$. The quantities $k = \omega\sqrt{\mu_0\epsilon}$ and $\epsilon$ represent, respectively, the wave number and permittivity of the homogeneous medium. Now, representing (5) with its plane wave spectrum and imposing the boundary condition of electric and magnetic fields at the half-space boundary, we get the transmission coefficient ($\mathbf{T}^{\perp}$) as

$$\mathbf{T}^{\perp} = \frac{2k_{y_0}}{k_{y_0} + k_{y_b}}e^{jk_{y_0}y_s}, \tag{6}$$

where $k_{y_i} = \sqrt{k_i^2 - k_x^2}$ with $i = \{0, b\}$. Referring to the geometry shown in Figure 1, $y_s = 0$. Therefore, using (6) and the stationary phase approximation, (5) has been modified to develop the analytical expression for the incident electric field in the lower half-space ($\underline{r} \in \mathcal{D}$). So,

$$E_{inc,z}^{soil} = \frac{-I_0 k_0^2}{4\omega\epsilon_0} \frac{2k_b\cos\theta_s}{k_b\cos\theta_s + \sqrt{k_0^2 - k_b^2\sin^2\theta_s}} H_0^{(2)}(k_b|\underline{r} - \underline{r}_s|). \tag{7}$$

Where $\sin\theta_s$ is expressed as

$$\sin\theta_s = \frac{(x - x_s)}{\sqrt{(x - x_s)^2 + y^2}}. \tag{8}$$

It is important to note that a closed-form expression cannot be obtained in those cases where the source is not located at the half-space interface and (or) when the object is sufficiently close to the source. They are expressed in terms of integral representation in those cases as given in (9), and they need to be solved numerically.

$$E_{inc,z}^{soil} = -\frac{I_0 k_0^2}{4\omega\epsilon_0}\frac{1}{\pi}\int_{-\infty}^{\infty} \frac{2e^{jk_{y_0}y_s}}{k_{y_0} + k_{y_b}} e^{-jk_{y_b}y} e^{jk_x(x - x_s)} dk_x. \tag{9}$$

### B. SCATTERED FIELD DUE TO A SINGLE PEC CYLINDER BURIED IN LOWER HALF-SPACE

A half-space scenario shown in Figure 2 has been considered for this case. A cylindrical PEC (which has a circular

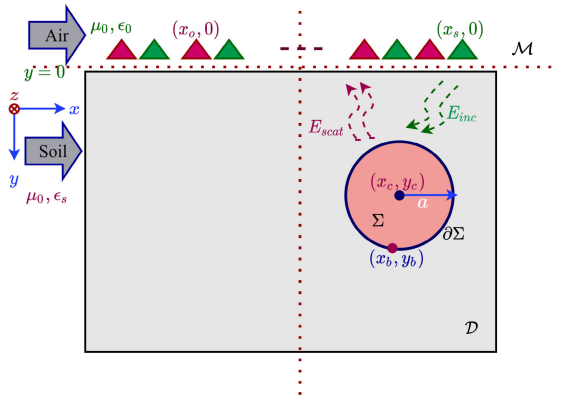


**FIGURE 2.** Representation of buried PEC in half-space.

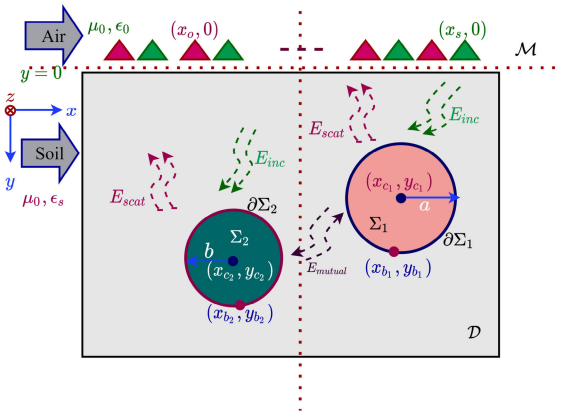


**FIGURE 3.** Investigation scenario for two PEC scatterers.

cross-section in two-dimension) having the center at $(x_c, y_c)$ with cross-sectional radius $a$ is buried in the soil. The region $y < 0$ represents the air, and $y > 0$ indicates the non-magnetic background with complex relative permittivity $\epsilon_s$. As the buried anomalous object is a PEC, the tangential component of the electric field will be zero at the boundary of the PEC $(x_b, y_b) \in \partial\Sigma$. Thus, representing $\underline{r}_b = x_b\hat{a}_x + y_b\hat{a}_y$ and $\underline{r}_c = x_c\hat{a}_x + y_c\hat{a}_y$ as the respective position vectors of $(x_b, y_b)$ and $(x_c, y_c)$, we can conclude that $|\underline{r}_b - \underline{r}_c| = a$. Now, as there is no electric field inside the PEC, the scattered field will always be outgoing from the periphery of the cylinder. Thus, the scattered field can be expressed mathematically and given as

$$E^{soil}_{scat,z} = \mathbf{C}H^{(2)}_0(k_b|\underline{r} - \underline{r}_c|). \tag{10}$$

Here, $\mathbf{C}$ in (10) has been computed by imposing the electric field boundary condition at the periphery of the PEC. So,

$$\mathbf{C} = -\frac{-I_0k_0^2}{4\omega\epsilon_0}\frac{2k_b\cos\theta_b}{k_b\cos\theta_b + \sqrt{k_0^2 - k_b^2\sin^2\theta_b}} \times \frac{H^{(2)}_0(k_b|\underline{r}_b - \underline{r}_s|)}{H^{(2)}_0(k_b a)}. \tag{11}$$

Here, the parameter $\sin\theta_b$ in (11) can be calculated from (8) with replacing $(x, y)$ by $(x_b, y_b)$. The induced current density generates the scattered electric field, and the induced current density is dependent on the strength of the field incident on the scatterer. Due to the presence of the half-space, there will be a reflection of the scattered field at the interface. Therefore, the scattered field reflected from the interface will be of reduced amplitude than the original one. Hence, at the vicinity of the scatterer, the amplitude of the scattered electric field is insignificant compared to the sum of the amplitude of the incident and that of the scattered electric field. Therefore, the scattered field reflected from the interface can be neglected under this situation. Thus, it is essential to note that while deriving the expression for $\mathbf{C}$, the portion of the scattered electric field backpropagated from the half-space interface has been ignored. The scattered electric field transmitted from the lower half-space to the air will be measured by receiving antennas positioned at the half-space boundary.

Hence, by imposing the field boundary conditions on the electric and magnetic fields and with the help of the stationary phase approximation, we can determine the scattered electric field at the interface as

$$E^{air}_{scat,z} = \mathbf{C}\frac{2k_b\cos\theta_c}{k_b\cos\theta_c + \sqrt{k_0^2 - k_b^2\sin^2\theta_c}}H^{(2)}_0(k_b|\underline{r}_0 - \underline{r}_c|), \tag{12}$$

where

$$\sin\theta_c = \frac{(x_0 - x_c)}{\sqrt{(x_0 - x_c)^2 + y_c^2}}. \tag{13}$$

From the above analysis, for each point on the boundary of the PEC, (11) can be evaluated. Thus, at any specific observation point, the effective scattered electric field has been calculated by superpositioning those originating from each point on the boundary. Due to PEC, there is a mismatch of magnetic fields at the boundary, which induces an electric current density at the periphery of the PEC. This induced current density is causing the scattered electric and magnetic fields in the investigation domain.

### C. SCATTERED FIELD DUE TO A SINGLE DIELECTRIC CYLINDER BURIED IN LOWER HALF-SPACE

The investigation domain shown in Figure 2 has also been considered for the case of the dielectric. Here, instead of a PEC, a dielectric cylinder with cross-sectional radius $a$ is buried at the lower half-space. The center of the dielectric is located at $(x_c, y_c)$ and the cylinder has a relative permittivity of $\epsilon_d$, a complex quantity in general. The rest of the assumptions on the investigation scenario remain unaltered as described in the case of PEC. The calculation of the scattered electric field due to the buried dielectric cylinder is not as straightforward as it had been for the PEC. There will be some amount of electric field inside the dielectric cylinder. Referring to [40], [41] the electric field transmitted inside the dielectric and that scattered outside can be represented by (16) and (17), respectively. Therefore,

$$E^{diel}_{tr,z} = \mathbf{T_d}J_0(k_d|\underline{r} - \underline{r}_c|); \quad \underline{r} \in \Sigma, \tag{16}$$

and $E^{soil}_{scat,z} = \Gamma_{\mathbf{d}} H_0^{(2)}(k_b|\underline{r} - \underline{r}_c|) \quad \underline{r} \in \mathcal{D};\ \underline{r} \notin \Sigma.$ (17)

The parameters $\mathbf{T_d}$ and $\Gamma_{\mathbf{d}}$ in (16) and (17), respectively, denote the amplitudes of the respective fields. Similar to the assumption made in the case of PEC, here also, we are assuming that the contribution of the scattered electric field flowing back from the air-soil interface is negligible compared to the original one. Thus, imposing the field boundary conditions at the dielectric soil boundary, we can deduce the analytical expressions for $\mathbf{T_d}$ and $\Gamma_{\mathbf{d}}$. Therefore, doing so, we get (14) and (15), as shown at the bottom of the page. The prime in the Hankel function and Bessel's function denotes their corresponding first derivative with respect to $\underline{r}$. The derivation of the expression for $\sin\theta_b$ in (14) and (15) is similar to that in the case of PEC. Thus, using (12) and (13), we can derive the expression for the scattered electric field at the air-soil interface. Hence,

$$E^{air,diel}_{scat,z} = \Gamma_{\mathbf{d}} \frac{2k_b \cos\theta_c}{k_b \cos\theta_c + \sqrt{k_0^2 - k_b^2 \sin^2\theta_c}} H_0^{(2)}(k_b|\underline{r}_0 - \underline{r}_c|). \tag{18}$$

As mentioned in the case of the PEC scatterer, here also the effective scattered field is the superposition of the fields contributed by each point on $\partial\Sigma$ of the dielectric.

### D. SCATTERED FIELD DUE TO TWO PEC CYLINDERS BURIED IN LOWER HALF-SPACE

So far in the previous subsections, we have derived the mathematical equations for the scattered electric fields measured in the half-space boundary when a single scattering object is buried in the lower half-space. In this subsection, we will derive the expressions for the scattered electric fields both at the air-soil interface as well as in the lower half-space when two PEC cylinders are buried. Let us refer to the investigation scenario represented by Figure 3. Two PEC cylinders ($\Sigma_1$ and $\Sigma_2$) with different cross-sectional radii are positioned arbitrarily at $(x_{c_1}, y_{c_1})$ and $(x_{c_2}, y_{c_2})$. The quantities $r_{c_1}$ and $r_{c_2}$ denote the position vectors corresponding to the center of the PEC cylinders. Extending the similar concepts used for the case of a single cylindrical object here, we can calculate the effective scattered electric fields contributed by these two cylinders independently. Thus, extending (10) for the case of two cylinders, we get

$$E^{soil}_{scat,z} = \mathbf{C_1} H_0^{(2)}(k_b|\underline{r} - \underline{r}_{c_1}|) + \mathbf{C_2} H_0^{(2)}(k_b|\underline{r} - \underline{r}_{c_2}|). \tag{19}$$

By following the standard procedure of matching the fields at the boundaries of the soil and the respective PECs, we can deduce the mathematical expressions for the quantities $\mathbf{C_1}$ and $\mathbf{C_2}$. Let us represent the generic points $(x_{b_1}, y_{b_1}) \in \partial\Sigma_1$ and $(x_{b_2}, y_{b_2}) \in \partial\Sigma_2$ as the points on the peripheries of the respective PEC targets. Also, the position vectors of the respective boundary points are represented as $\underline{r}_{b_1}$ and $\underline{r}_{b_2}$. Now, similar to the situation assumed for the single PEC or dielectric case, here also,we have chosen the boundary points in such a way that it satisfies $|\underline{r}_{b_1} - \underline{r}_{c_1}| = a$ and $|\underline{r}_{b_2} - \underline{r}_{c_2}| = b$. It is important to note that while imposing the boundary conditions at the boundary of the first cylinder, we are considering the effect of the scattered field due to the second one and vice-versa. In this way, the mutual interaction of the fields is accounted into the model [refer to (25) and (26)]. Hence, solving the respective equations generated from matching the electric fields at the boundaries we get,

$$\mathbf{C_1} = \frac{R_2 Q_1 - R_1 Q_2}{P_1 Q_2 - P_2 Q_1}, \tag{20}$$

$$\mathbf{C_2} = \frac{R_2 P_1 - R_1 P_2}{P_2 Q_1 - P_1 Q_2}, \tag{21}$$

where the quantities in (20) and (21) are given in (22)-(27).

$$R_1 = \frac{-I_0 k_0^2}{4\omega\epsilon_0} \frac{2k_b \cos\theta_{b_1}}{\sqrt{k_0^2 - k_b^2 \sin^2\theta_{b_1}} + k_b \cos\theta_{b_1}} \times H_0^{(2)}(k_b|\underline{r}_{b_1} - \underline{r}_s|). \tag{22}$$

$$R_2 = \frac{-I_0 k_0^2}{4\omega\epsilon_0} \frac{2k_b \cos\theta_{b_2}}{\sqrt{k_0^2 - k_b^2 \sin^2\theta_{b_2}} + k_b \cos\theta_{b_2}} \times H_0^{(2)}(k_b|\underline{r}_{b_2} - \underline{r}_s|). \tag{23}$$

$$P_1 = H_0^{(2)}(k_b a). \tag{24}$$

$$P_2 = H_0^{(2)}(k_b|\underline{r}_{b_2} - \underline{r}_{c_1}|). \tag{25}$$

$$Q_1 = H_0^{(2)}(k_b|\underline{r}_{b_1} - \underline{r}_{c_2}|). \tag{26}$$

$$Q_2 = H_0^{(2)}(k_b b). \tag{27}$$

The expressions corresponding to $\sin\theta_{b_1}$ and $\sin\theta_{b_2}$ have been derived with the help of (8) by replacing $(x, y)$ with $(x_{b_1}, y_{b_1})$ and $(x_{b_2}, y_{b_2})$, respectively. Finally, with the help of stationary phase approximation, the scattered electric field measured at the air-soil interface can be expressed as

$$E^{air}_{scat,z} = \frac{2k_b \cos\theta_{c_1}}{\sqrt{k_0^2 - k_b^2 \sin^2\theta_{c_1}} + k_b \cos\theta_{c_1}} H_0^{(2)}(k_b|\underline{r}_o - \underline{r}_{c_1}|)$$

$$\mathbf{T_d} = \frac{-I_0 k_0^2}{4\omega\epsilon_0} \frac{2k_b \cos\theta_b}{\sqrt{k_0^2 - k_b^2 \sin^2\theta_b} + k_b \cos\theta_b} \frac{\sqrt{\epsilon_b} H_0^{\prime(2)}(k_b|\underline{r}_b - \underline{r}_s|) H_0^{(2)}(k_b a) - H_0^2(k_b|\underline{r}_b - \underline{r}_s|)\sqrt{\epsilon_b} H_0^{\prime(2)}(k_b a)}{\sqrt{\epsilon_b} H_0^{\prime(2)}(k_b a) J_0(k_d a) - \sqrt{\epsilon_d} J_0'(k_d a) H_0^{(2)}(k_b a)} \tag{14}$$

$$\Gamma_{\mathbf{d}} = \frac{-I_0 k_0^2}{4\omega\epsilon_0} \frac{2k_b \cos\theta_b}{\sqrt{k_0^2 - k_b^2 \sin^2\theta_b} + k_b \cos\theta_b} \frac{\sqrt{\epsilon_b} H_0^{\prime(2)}(k_b|\underline{r}_b - \underline{r}_s|) J_0(k_d a) - \sqrt{\epsilon_d} H_0^2(k_b|\underline{r}_b - \underline{r}_s|) J_0'(k_d a)}{\sqrt{\epsilon_b} H_0^{\prime(2)}(k_b a) J_0(k_d a) - \sqrt{\epsilon_d} J_0'(k_d a) H_0^{(2)}(k_b a)} \tag{15}$$

$$\times \mathbf{C_1} + \frac{2k_b \cos\theta_{c_2}}{\sqrt{k_0^2 - k_b^2 \sin^2\theta_{c_2}} + k_b \cos\theta_{c_2}} \times \mathbf{C_2} H_0^{(2)}(k_b|\underline{r}_o - \underline{r}_{c_2}|). \quad (28)$$

The values of $\sin\theta_{c_1}$ and $\sin\theta_{c_2}$ in (28) can be obtained from (13) by replacing $(x_c, y_c)$ with $(x_{c_1}, y_{c_1})$ and $(x_{c_2}, y_{c_2})$, respectively. To get a more general idea to solve scattered electric fields for multiple scattering objects in a homogeneous unbounded medium, interested readers may follow [42].

## III. ESTIMATION OF SIZE OF THE SCATTERER THROUGH INVERSION

In this section, we will propose an algorithm to estimate the size and type (either a dielectric or a PEC) of the scatterers present in the half-space. The algorithm needs the location of the scattering object as one of the inputs. This information about the location of the scattering object has been obtained through a qualitative inversion. Therefore, different linear imaging methods have been discussed first, followed by the proposition of the algorithm for estimating the size and type of the unknown scatterer present in half-space.

### A. QUALITATIVE INVERSION MODELS

Now referring to (4), let us represent the first quantity $\frac{\epsilon_r - \epsilon_b}{\epsilon_b}$ in the integral as $\chi$. Hence, using the assumption that the total field is the sum of incident and the scattered one, (4) can be written as

$$E_{scat}(\underline{r}) = k_b^2 \int_{\mathcal{D}} \chi(\underline{r}')G_{21}(\underline{r}, \underline{r}') \times \left[ E_{inc}(\underline{r}') + k_b^2 \int_{\mathcal{D}} G_{22}(\underline{r}', \underline{\lambda})\chi(\underline{\lambda})E_{tot}(\underline{\lambda})d\underline{\lambda} \right] d\underline{r}'. \quad (29)$$

#### 1) GENERALIZED LINEARIZATION WITH BORN APPROXIMATION

Equation (29) being non-linear, needs to solve iteratively. However, it can be simplified by neglecting the integral with respect to the running variable $\lambda$, leading to the very popular procedure BA [13]–[16]. Therefore, under the BA

$$F(\chi) = k_b^2 \int_{\mathcal{D}} \chi(\underline{r}')G_{21}(\underline{r}', \underline{r}_0)E_{inc}(\underline{r}')d\underline{r}' = E_{scat}(\underline{r}_o). \quad (30)$$

Here, the operator $F$ is square integrable, mapping the investigation domain to the measurement one, i.e $F : L^2(\mathcal{D}) \rightarrow L^2(\mathcal{M})$. Therefore, looking into (30), we can see that, in order to carry out the inversion, one needs to know the expression for Green's function of the investigation domain along with that of the incident electric field. Several kinds of researches have been carried earlier to explore the scope of BA and the factors influencing its performance. Hence, they are not discussed in detail.

#### 2) INVERSION BASED ON CURRENT DENSITY RECONSTRUCTION (CDR)

With reference to (2), we have seen that the scattered electric field due to an anomalous target is a function of the induced current density and Green's function of the medium. Thus, with the proper model of Green's function of a particular geometry only, fields radiated by an arbitrary current source can be computed. Hence, the right-hand side (RHS) of (2) can be defined as an operator that converts the induced current density into the radiated fields without loss of generality. So, instead of reconstructing the contrast, reconstruction of the current density can provide the position of the scatterer. Thus, for the half-space geometry,

$$F_i\{J(\underline{r})\} = \int_{\mathcal{D}} J(\underline{r})G_{21}(\underline{r}_0, \underline{r})d\underline{r} = E_{scat}(\underline{r}_o), \quad (31)$$

where $\underline{r}_o \in \mathcal{M}$. As the integral is square integrable for bounded values of $J$, the operator can be written as $F_i : L^2(\mathcal{D}) \rightarrow L^2(\mathcal{M})$. This procedure is similar to the concept used in BA based linearization; however, it is different from the BA. Comparing (31) with (30), it can be concluded that based on the mathematical complexity and computational complexity, reconstruction of the current density instead of the contrast function is advantageous as it avoids the dependency on the electric field in the investigation domain. Although a brief discussion regarding the CDR is available in [1], the applicability of this method is merely reported in recent studies. One of the probable reasons is that both the classical BA and CDR result in similar images of the unknown scatterer.

Referring to [40], the analytical expression for $G_{21}(\underline{r}_0, \underline{r}')$ is

$$G_{21}(\underline{r}_0, \underline{r}') = \frac{k_b \cos\theta_o}{\sqrt{k_0^2 - k_b^2 \sin^2\theta_o} + k_b \cos\theta_o} H_0^{(2)}(k_b|\underline{r}_o - \underline{r}'|); \quad \underline{r}_o \in \mathcal{M}; \quad \underline{r}' \in \mathcal{D}. \quad (32)$$

So, by inversion of the integral in (31), the current density causing the scattered electric field can be reconstructed.

#### 3) LINEAR SAMPLING METHOD

As mentioned earlier, the LSM is one of the qualitative methods used to determine the geometrical boundary of the scatterer. According to the LSM, the support of the unknown scatterer is estimated by a far-field operator given in (33) when the uniform plane wave of unity amplitude from the different directions illuminate the investigation domain. Thus,

$$F_L\{\zeta(\underline{r}_p)\} = \int_0^{2\pi} E_{scat}^{\infty}(\hat{r}, \phi)\zeta(\underline{r}_p, \phi)d\phi = G^{\infty}(\underline{r}_p). \quad (33)$$

Here, $E_{scat}^{\infty}(\hat{r}, \phi)$ in (33) represents the scattered far-field measured in the measurement domain in the radial direction

pointed by unit vector $\hat{r}$ when a plane wave from the direction $\phi$ is incident on the investigation domain. Similarly, $G^{\infty}(\underline{r}_p)$ represents the far-field radiated by the point source located at $\underline{r}_p$. The quantity $\zeta(\underline{r}_p, \phi)$ is termed as the support indicator whose $L_2-$norm ($||\zeta(\underline{r}_p, \phi)||^2$) becomes unbounded if $\underline{r}_p$ does not lie within the unknown scatterer. However, in the case of the half-space geometry, the classical LSM needs alteration. Hence, the modified operator can be written as (concerning Figure 1) [27]

$$F_{HL}\{\zeta(\underline{r}_p, x_s)\} = \int_{\mathcal{M}} E_{scat}(x_0, x_s)\zeta(\underline{r}_p, x_s)dx_s = G_{21}(\underline{r}_p). \tag{34}$$

Therefore, by solving the $L_2-$norm for each $\underline{r}_p \in \mathcal{D}$, we may get the shape and position of the scatterer.

### B. REGULARIZED INVERSION

One can determine the unknowns in the operators $F$ and $F_i$, given in (30) and (31), respectively, by Method of Moment (MoM), achieved through discretizing the investigation domain [43]. It had been shown in previous literature that these operators are not directly invertible and require a regularized solution. Truncated Singular Value Decomposition (TSVD) based regularized inversion is one of its kind that is commonly used by many researchers. Although there are many research pieces, readers can refer [15], [16] for an idea. Detail discussion regarding the same has been kept out of the scope of the present discussion.

### C. EXTENSION OF QUALITATIVE IMAGING TO ESTIMATE THE SIZE AND TYPE OF THE SCATTERER

Once the information about the location of the target is retrieved from the map of the current density or the distribution of the contrast function in the investigation domain, the following procedure can be adopted for inferring the approximate diameter and type of the target:

1) From the inversion results, determine the number of targets and respective coordinate values of the center of the targets.
2) Choose a set of values for the approximate radius (an idea of selecting the range of radius can be obtained from the approximate spread of the current densities).
3) For a single target, for the chosen set of radii values and making a fair guess on the relative permittivity of the target, respective analytical formulations given in Section-II can be used.
4) For more than two targets, the process becomes further complicated as the field is influenced by the coordinate values of the respective targets and their radii.
5) By choosing the appropriate formulation, the best match between the predicted scattered field and that of the measured scattered field can be achieved for a specific value of radius. The minimum value of the Mean Square Error (MSE) can be considered as a metric for determining the best fit.

The proposed procedure is similar to that used in solving the non-linear inversion problems. However, the proposed one is computationally simpler than the non-linear inversion ones as it can take advantage of the developed closed-form expressions of the scattered electric field instead of solving the complex forward scattering problems. Estimation of the actual complexity of the proposed algorithm has been kept out of the scope of the present study.

## IV. NUMERICAL EXPERIMENTS

In this section, we will show the results of the qualitative inversion, followed by the performance of the proposed algorithm. In our study, instead of using the numerical solution, we have used the analytical expressions to generate the scattered electric field. Therefore, the results of the inversion using these scattered field data also help to prove the validity of the developed scattered field data. As an explanation, if the inversion of electric field data, predicted by the analytical model of a single PEC scatterer, results in a single object then, we can claim the model as a valid one. The same concept can be extended for the other cases too. It is important to note that all the results shown in the subsequent stages are generated with a high signal to noise ratio situation (> 30 dB).

### A. IMPLEMENTATION OF LINEAR INVERSION METHODS

It is important to note that as the constitutive parameter of the buried target is unknown, BA based linearized inversion scheme is considered. It is also essential to be remembered that the LSM is applied at 0.5 GHz throughout the cases.

#### 1) RECONSTRUCTION OF SINGLE PEC CYLINDER

For reconstructing a PEC cylinder, the investigation domain shown in Figure 2 has been considered. The investigation domain has a size of 1 m $\times$ 1 m, and it is filled with a lossless material with relative permittivity of 2.0. A PEC scatterer with a cross-sectional diameter of 14 cm is coordinated arbitrarily at different positions in the lower-half space of the investigation domain. An array of 60 transceiving antennas has been placed along the boundary of the half-space. As literature reveals that the BA based inversion works well when the multi-monostatic multi-frequency configuration is considered; therefore, here also the same is used [14]–[16]. For BA, the operating frequency range has been selected as 0.4 GHz to 0.6 GHz with ten uniform frequency steps.

However, for the CDR and LSM, the multi-static single frequency configuration has been considered. In this configuration, at a particular instant, one antenna (at a specific position) among the arranged antennas acts as a source, and the remaining act as receivers. We have seen during the development of the forward scattering model that the position of the source influences the scattered electric field; therefore, in another way, we can claim that the position of the source also affects the current density induced at the location of the scatterer. Hence, at each of the positions of the source, the received fields are inverted. In the end, the individual inversion results are averaged to get the final one. The results are

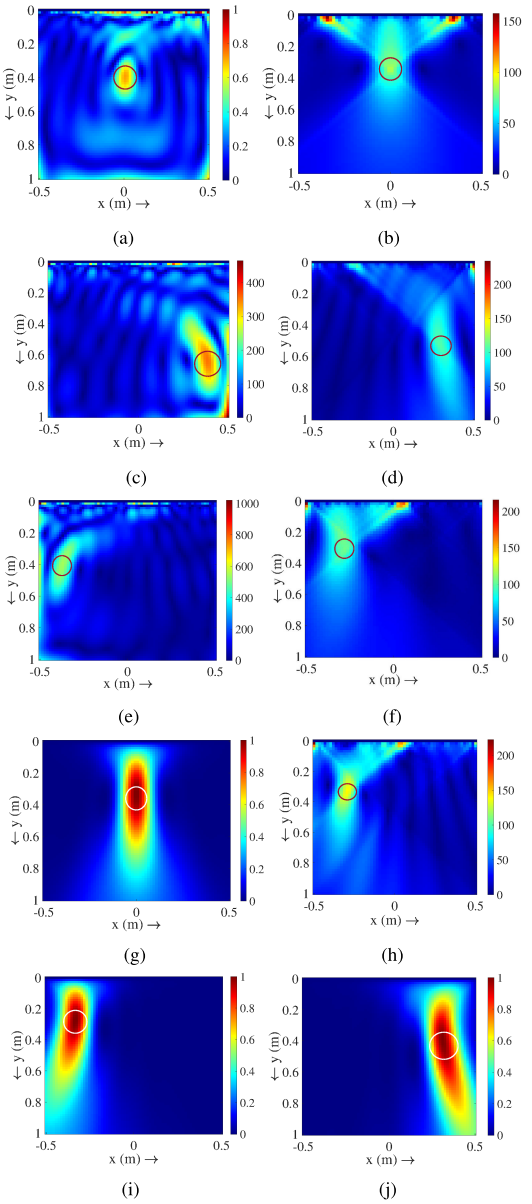


**FIGURE 4.** Reconstruction of PEC target: (a) with BA (target located at (0, 0.35)), (b) with CDR at 0.5 GHz (target located at (0, 0.35)), (c) with BA (target located at (0.35, 0.55)), (d) with CDR at 1.2 GHz (target located at (0.35, 0.55)), (e )with BA (target located at (−0.35, 0.35)), (f) with CDR at 0.5 GHz (target located at (−0.35, 0.35)), (g) with LSM (target located at (0, 0.35)), (h) with CDR at 1.2 GHz (target located at (−0.35, 0.35)), (i) with LSM (target located at (−0.35, 0.35)) and (j) with LSM (target located at (0.35, 0.55)).

shown in Figure 4. Comparing Figure 4(a) with Figure 4(b), Figure 4(c) with Figure 4(d), and Figure 4(e) with Figure 4(f), it can be concluded that the images constructed with BA place the PEC target into a deeper level as compared to their actual location. On the contrary, the images created with CDR based inversion place the scatterers to their corresponding actual locations accurately. Hence, the CDR based inversion is proven more suitable in the case of imaging a single PEC target. It is also worth observing that the modified LSM in the half-space could not provide shape of scatterer. Similar result was also found in [25], [27]. The frequency dependency of

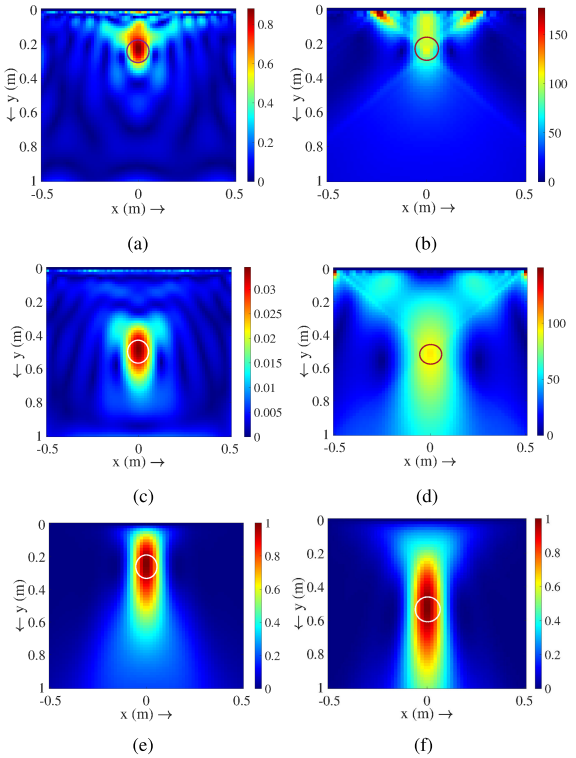


**FIGURE 5.** Reconstruction of a dielectric target: (a) with BA (target located at (0, 0.25)), (b) with CDR at 0.5 GHz (target located at (0, 0.55)), (c) with BA (target located at (0, 0.55)), (d) with CDR at 0.5 GHz (target located at (0, 0.55)), (e) with LSM (target located at (0, 0.25)) and (f) with LSM (target located at (0, 0.55)).

the CDR based inversion method has been studied for this case. Comparing Figure 4(f) and Figure 4(h), we can observe that as the frequency of operation increases, the spread of the current density in the vicinity of the scattering object gets reduced, providing a better reconstruction. It can also be pointed that distortion in retrieving location information provided by BA and LSM is noticed.

It was already said earlier that the conventional BA is the most popular one, and many researchers had applied it in half-space. A detailed study on the effect of the measurement configurations on BA is available in [44]. The study shown in [44] had considered a weak scattering object only. An analysis of the performance of BA based reconstruction while both the strong and weak scatterers are embedded in half-space was reported in [4]. The applicability of linear inversion on the experimental data is available in [2], [45]. Hence, from the previous experiments, it can be seen that the conventional BA can only localize the targets, and the results shown in Figure 4(a) - Figure 4(f) corroborate the earlier findings for multi-monostatic multi-frequency case.

### 2) RECONSTRUCTION OF SINGLE DIELECTRIC CYLINDER

An investigation domain that was considered in reconstructing the PEC cylinder has been used for reconstructing the dielectric. The dimension of the investigation domain, constitutive parameter of the background medium, and the arrangement of antennas remain unaltered as it was in the case of

PEC. In this case, instead of a PEC cylinder, a lossy dielectric cylinder ($\epsilon_d = 8.0 - j0.02$) of a cross-sectional diameter of 14 cm is assumed to be located at the lower half-space. Figure 5 shows the reconstruction results obtained through the previously mentioned inversion methods. Similar to the earlier case, for BA, the frequency range of 0.4 GHz to 0.6 GHz is used with ten uniform steps.

In the case of reconstruction of single PEC material, we have examined the frequency dependency of the CDR based inversion method. Here, in this case, also, similar behavior has been noticed. Therefore, the results for the same are not shown. From Figure 5, it can be concluded that all the methods can unambiguously identify the position of the dielectric target. However, in the LSM based reconstruction, the approximate size of the target increases mainly due to the half-space, causing the limitation in the illumination. An important observation can be pointed here that, in the case of reconstruction of the buried single dielectric, the BA based inversion works better compared to the case of the single PEC as the inversion model suits better for a dielectric. As observed in the case of reconstructing a PEC, in this case also, results are comparable to those shown in [2], [4], [44].

#### 3) RECONSTRUCTION OF TWO PEC CYLINDERS

The generic half-space investigation geometry shown in Figure 3 has also been considered in the case of reconstruction. The size of the investigation domain is 1 m × 1 m, and it is filled with a lossless dielectric of relative permittivity 2.0. Two PEC cylinders with the same diameters of 0.14 m are coordinated arbitrarily. The multi-static single frequency configuration has been used in the inversion. The inversion results are shown in Figure 6. As there is more than one target in the investigation domain, there will be mutual scattered electric fields in between the targets. Thus, to verify this effect, the targets have been placed closely in one case, and in another case, they are kept away from each other. As done in earlier cases, a frequency range of 0.4 GHz to 0.6 GHz with ten equispaced steps has been used for BA based reconstruction. Referring to Figure 6(a), we can observe that a ghost target has appeared in between the actual PEC targets when BA based reconstruction is applied. A similar phenomenon was reported in [4] when the scatterers are positioned close to each other. Referring to Figure 6(b), we can see that the appearance of the ghost targets is insignificant when the CDR based reconstruction is applied at 0.5 GHz. However, the effect becomes prominent when the frequency of operation is increased to 1.2 GHz (Figure 6(e)). The probable reason behind this is the effect of the scattered mutual field in between the targets, although finding the actual reasons needs further investigation. It is essential to observe that when the inter target distance is kept sufficiently large, the ghost targets in the reconstructed image disappear (refer to Figure 6(c), Figure 6(d), and Figure 6(f)). Although the performance of the LSM is poor in the case of a half-space geometry, the problem of ghost targets is not there in the case of LSM based reconstruction even when inter target distance is small.

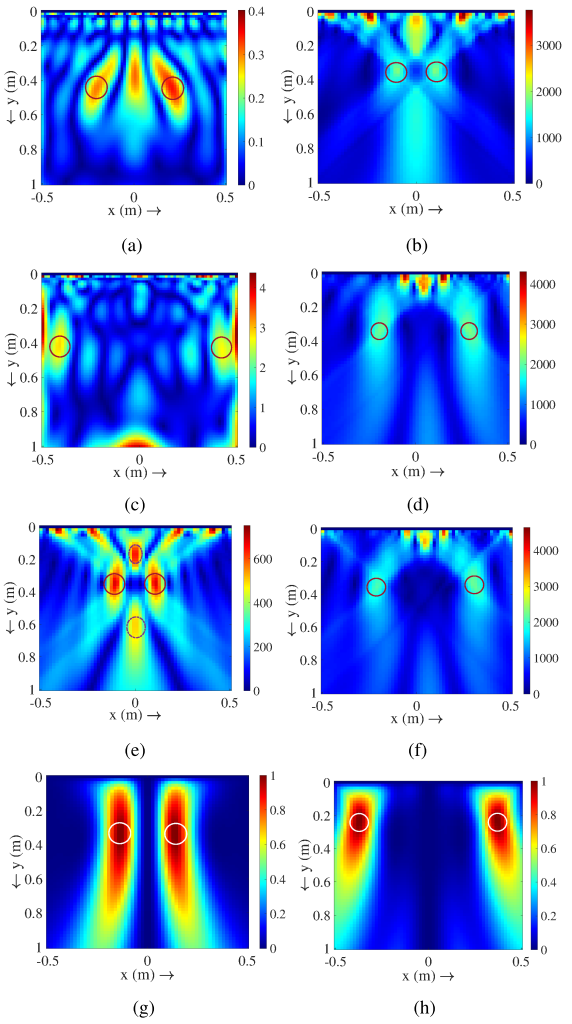


**FIGURE 6.** Reconstruction of two PEC targets: (a) with BA (target located at (−0.2, 0.4) and (0.2, 0.4) ), (b) with CDR at 0.5 GHz (target located at (−0.15, 0.35) and (0.15, 0.35)), (c) with BA (target located at (−0.4, 0.35) and (0.4, 0.35)), (d) with CDR at 0.5 GHz (target located at (−0.2, 0.35) and (0.3, 0.35)), (e) with CDR at 1.2 GHz (target located at (−0.15, 0.35) and (0.15, 0.35)), (f) with CDR 1.2 GHz (target located at (−0.2, 0.35) and (0.3, 0.35)), (g) with LSM (target located at (−0.15, 0.35) and (0.15, 0.35)), and (h) with LSM (target located at (−0.4, 0.35) and (0.4, 0.35)). The boxes and circles indicate the existence of targets and ghosts only, do not carry any information on shape and size.

### B. RETRIEVAL OF SIZE OF THE BURIED OBJECTS

In this subsection, the performance of the proposed method in determining the size and type of the buried targets is discussed. In the earlier subsection we have proved the correctness of the developed analytical expression by localizing the targets through inversion. Also, referring to Figure 4 - Figure 6, we can conclude that CDR, being simple, is well-suited for all cases. All the inversion methods discussed here lead to localization only. Therefore, considering the superiority, information obtained from CDR is fed to the proposed algorithm. It can be noted that throughout the analysis, the operating frequency of the source is chosen as 0.5 GHz. The multi-static measurement configuration with the source located at (0, 0) has been considered while determining the best fit of the scattered electric fields.

### 1) CASE-A: SINGLE PEC

In this case, we will consider two examples where the target is located in two different positions to verify the performance of the size retrieval method on the variability of depth. Let us refer to the results shown in Figure 4(b) and Figure 4(d). The reason behind choosing these two cases is that one of them is a shallow target, and another is a deeply-buried one. Referring to Figure 4(b), by manual inspection, the coordinate of the buried object is determined as $(0.007, 0.347)$ m. Similarly, following the same process, the coordinate of the center of the target shown in Figure 4(d) is obtained as $(0.340, 0.522)$ m. Now using (12), the scattered electric fields have been computed for different radii of the cylindrical object centered at the respective coordinates. The results are shown in Figure 7. Figure 7(a) and Figure 7(b) show the variation of the MSE with different values of the radii chosen for the target centered at $(0, 0.35)$ m and $(0.35, 0.55)$ m, respectively. From the figures, the lowest value of MSE for the individual cases has been found, and the radii values are respectively 0.079 m and 0.071 m for the shallow and deep targets. A comparison of the actual and predicted fields for both the shallow and deep targets with the retrieved radius values is shown in Figure 7(e) and Figure 7(f), respectively. The peripheries of the reconstructed targets are shown in Figure 7(c) and Figure 7(d). Using the analytical expression, the set of values $(x, y)$, constituting the radius of the cylindrical targets, is filled with a constant value to represent the periphery. Therefore, the colorbars shown in Figure 7(c) and Figure 7(d) do not carry any useful information.

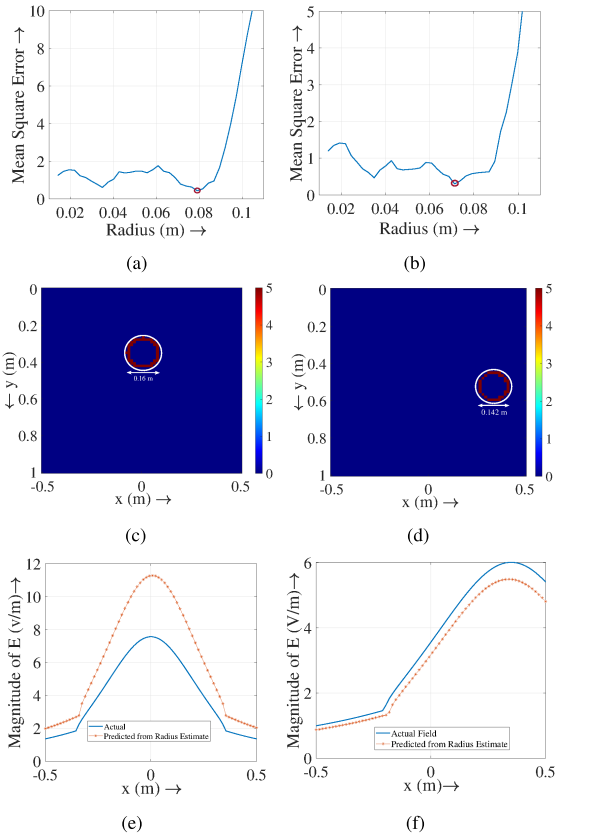


**FIGURE 7.** (a) Variation of MSE with radius for the target centered at (0, 0.35), (b) Variation of MSE with radius for the target centered at (0.35, 0.55), (c) Retrieved diameter of the shallow target, (d) Retrieved diameter of the deep target, (e) Actual and predicted field for the shallow target and (f) Actual and predicted field for the deep target.

### 2) CASE-B: SINGLE DIELECTRIC TARGET

We have already seen the performance of the size retrieval on the depth of the buried target. From the results (referring to Figure 7), it is found that it works well for a shallow target as well as for the target buried deep. Thus, in the case of dielectric, we considered a single example. Let us refer to Figure 5(d) and determine the center of the target by manual inspection. From Figure 5(d), the value of the center of the target has been found as $(0.008, 0.525)$ m. The variation in the MSE as a function of the radius of the cylinder is shown in Figure 8(a). It can be noted that for the validation purpose and also for simplicity, we have assumed the relative permittivity of the dielectric cylinder used in (18) is known beforehand. However, for the unknown targets, a similar procedure can be followed by updating the value of the relative permittivity of the dielectric target. From Figure 8(a), it can be observed that the minimum error occurs for the radius value 0.061 m; thus, it has been considered as the size of the cylindrical object. Figure 8(c) shows a comparison between the actual field and predicted field using the radius value as 0.061 m. Figure 8(e) shows the periphery of the reconstructed object for the dielectric cylinder.

### 3) CASE-C: TWO PEC CYLINDERS

In the previous subsection while studying the performance of the inversion schemes, we have found that some additional targets appear as ghosts for targets placed nearby to each other. Thus, we have chosen the case of the closely spaced targets to infer the size information and check the performance. Here, in this case, let us refer to Figure 6(b) and determine the coordinates of the center of the cylindrical objects. From the same, they have been noted as $(-0.152, 0.347)$ m and $(0.152, 0.347)$ m. The appearance of more than one cylinder in the reconstructed image of the current density makes it easier to choose the analytical expression. However, the presence of two objects with different radii further complicates the process of field matching. For simplicity, we have assumed that the targets have the same size, thereby reducing the complexity considerably. The variation of the MSE as a function of the radius for two PECs is shown in Figure 8(b). Compared to the other cases (Figure 7(a), Figure 7(b) and Figure 8(a)), it can be observed that the amount of error, in this case, is a bit higher. However, the error attains the minimum for the radius with a value of 0.08 m. It is important to note that the same procedure is also followed for other ghost objects in combination. However, those turned up into cases with very high MSE, are not shown here. A comparison between the actual and predicted field, and the retrieved periphery are shown in Figure 8(d) and Figure 8(f), respectively. An important observation has been made from this result that although a few ghost objects appeared in the reconstructed current density,

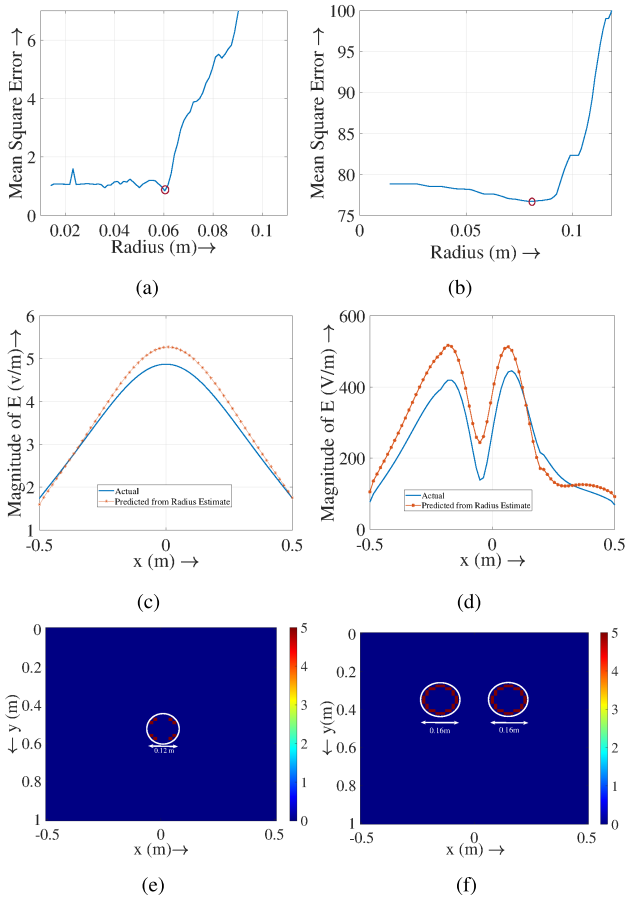


**FIGURE 8.** **(a) Variation of MSE as a function of radii for a single dielectric, (b) Variation of the MSE as function of radius for two PECs, (c) Comparison of scattered electric field for a single dielectric, (d) Comparison of the scattered electric field for two PECs, (e) Retrieved periphery for the dielectric and (f) Retrieved periphery for the two PECs.**

however, by an accurate analytical model, those objects have been suppressed successfully. As mentioned in the case of a single PEC, the colorbars in Figure 8(e) and Figure 8(f) do not carry any significant information.

## V. CONCLUSION

Based on the study we have carried so far, the following conclusive remarks can be drawn. Development of the analytic expression for the scattered electric field for the specific cases will be helpful to study the behavior of the scattered electric fields for different parameters influencing it. Also, in the case of inversion, the CDR based inversion method has proven to be most suitable in retrieving the qualitative information. The CDR based inversion is also more straightforward and effective as it avoids the direct utilization of the total electric field inside the investigation domain by incorporating it within the current density. Another significant utility of the CDR method is that it overcomes the effect of model-specific inversion and is found to be effective in reconstructing the dielectric and PEC. However, the BA based model is superior in reconstructing only the dielectric, and it introduces distortion while reconstructing the PEC. In addition, the developed electric field forward scattering models become effective in retrieving the size of the objects with great accuracy.

## REFERENCES


[1] M. Pastorino, *Microwave Imaging*. Hoboken, NJ, USA: Wiley, 2010.

[2] R. Solimene, A. Cuccaro, A. Dell'Aversano, I. Catapano, and F. Soldovieri, "Ground clutter removal in GPR surveys," *IEEE J. Sel. Topics Appl. Earth Observ. Remote Sens.*, vol. 7, no. 3, pp. 792–798, Mar. 2014.

[3] S. Maiti and A. Bhattacharya, "Microwave detection of respiration rate of a living human hidden behind an inhomogeneous optically opaque medium," *IEEE Sensors J.*, vol. 21, no. 5, pp. 6133–6144, Mar. 2021.

[4] F. Soldovieri and R. Solimene, "Through-wall imaging via a linear inverse scattering algorithm," *IEEE Geosci. Remote Sens. Lett.*, vol. 4, no. 4, pp. 513–517, Oct. 2007.

[5] S. Y. Semenov, A. E. Bulyshev, A. Abubakar, V. G. Posukh, Y. E. Sizov, A. E. Souvorov, P. M. Van Den Berg, and T. C. Williams, "Microwave-tomographic imaging of the high dielectric-contrast objects using different image-reconstruction approaches," *IEEE Trans. Microw. Theory Techn.*, vol. 53, no. 7, pp. 2284–2293, Jul. 2005.

[6] M. Salucci, G. Oliveri, and A. Massa, "GPR prospecting through an inverse-scattering frequency-hopping multifocusing approach," *IEEE Trans. Geosci. Remote Sens.*, vol. 53, no. 12, pp. 6573–6592, Dec. 2015.

[7] R. Chandra, H. Zhou, I. Balasingham, and R. M. Narayanan, "On the opportunities and challenges in microwave medical sensing and imaging," *IEEE Trans. Biomed. Eng.*, vol. 62, no. 7, pp. 1667–1682, Jul. 2015.

[8] T. Rubæ, P. M. Meaney, P. Meincke, and K. D. Paulsen, "Nonlinear microwave imaging for breast-cancer screening using Gauss–Newton's method and the CGLS inversion algorithm," *IEEE Trans. Antennas Propag.*, vol. 55, no. 8, pp. 2320–2331, Aug. 2007.

[9] M. Salucci, G. Oliveri, N. Anselmi, F. Viani, A. Fedeli, M. Pastorino, and A. Randazzo, "Three-dimensional electromagnetic imaging of dielectric targets by means of the multiscaling inexact-Newton method," *J. Opt. Soc. Amer. A, Opt. Image Sci.*, vol. 34, no. 7, pp. 1119–1131, Jul. 2017.

[10] L. Di Donato, M. Bevacqua, L. Crocco, and T. Isernia, "Inverse scattering via virtual experiments and contrast source regularization," *IEEE Trans. Antennas Propag.*, vol. 63, no. 4, pp. 1669–1677, Apr. 2015.

[11] A. Zakaria, C. Gilmore, and J. LoVetri, "Finite-element contrast source inversion method for microwave imaging," *Inverse Problems*, vol. 26, no. 11, pp. 1–21, 2010.

[12] G. Bozza and M. Pastorino, "An inexact Newton-based approach to microwave imaging within the contrast source formulation," *IEEE Trans. Antennas Propag.*, vol. 57, no. 4, pp. 1122–1132, Apr. 2009.

[13] W. Zhang and A. Hoorfar, "Two-dimensional diffraction tomographic algorithm for through-the-wall radar imaging," *Prog. Electromagn. Res. B*, vol. 31, pp. 205–218, 2011.

[14] F. Soldovieri, A. Brancaccio, G. Prisco, G. Leone, and R. Pierri, "A Kirchhoff-based shape reconstruction algorithm for the multimonostatic configuration: The realistic case of buried pipes," *IEEE Trans. Geosci. Remote Sens.*, vol. 46, no. 10, pp. 3031–3038, Oct. 2008.

[15] I. Catapano and L. Crocco, "A qualitative inverse scattering method for through-the-wall imaging," *IEEE Geosci. Remote Sens. Lett.*, vol. 7, no. 4, pp. 685–689, Oct. 2010.

[16] I. Catapano, A. Affinito, A. Del Moro, G. Alli, and F. Soldovieri, "Forward-looking ground-penetrating radar via a linear inverse scattering approach," *IEEE Trans. Geosci. Remote Sens.*, vol. 53, no. 10, pp. 5624–5633, Oct. 2015.

[17] R. Palmeri, M. T. Bevacqua, L. Crocco, T. Isernia, and L. Di Donato, "Microwave imaging via distorted iterated virtual experiments," *IEEE Trans. Antennas Propag.*, vol. 65, no. 2, pp. 829–838, Feb. 2017.

[18] L. Di Donato, R. Palmeri, G. Sorbello, T. Isernia, and L. Crocco, "A new linear distorted-wave inversion method for microwave imaging via virtual experiments," *IEEE Trans. Microw. Theory Techn.*, vol. 64, no. 8, pp. 2478–2488, Aug. 2016.

[19] S. Sun, B. J. Kooij, and A. G. Yarovoy, "Linearized 3-D electromagnetic contrast source inversion and its applications to half-space configurations," *IEEE Trans. Geosci. Remote Sens.*, vol. 55, no. 6, pp. 3475–3487, Jun. 2017.

[20] D. Colton, H. Haddar, and M. Piana, "The linear sampling method in inverse electromagnetic scattering," in *Proc. CBMS-NSF Regional Conf. Ser. Appl. Math.*, 2003, vol. 19, no. 80, pp. S105–S137s.

[21] S. N. Fata and B. B. Guzina, "A linear sampling method for near-field inverse problems in elastodynamics," *Inverse Problems*, vol. 20, no. 3, pp. 713–736, 2004.

[22] I. Catapano, L. Crocco, and T. Isernia, "On simple methods for shape reconstruction of unknown scatterers," *IEEE Trans. Antennas Propag.*, vol. 55, no. 5, pp. 1431–1436, May 2007.
[23] K. Agarwal, X. Chen, and Y. Zhong, "A multipole-expansion based linear sampling method for solving inverse scattering problems," *Opt. Exp.*, vol. 18, no. 6, pp. 6366–6381, 2010.
[24] F. Collino, M. B. Fares, and H. Haddar, "Numerical and analytical studies of the linear sampling method in electromagnetic inverse scattering problems," *Inverse Problems*, vol. 19, no. 6, pp. 1279–1298, Dec. 2003.
[25] W.-K. Park, "Application of linear sampling method for identifying location of small dielectric inhomogeneities in a half-space," in *Proc. Prog. Electromagn. Res. Symp.*, May 2017, pp. 2927–2930.
[26] I. Catapano, L. Crocco, and T. Isernia, "Improved sampling methods for shape reconstruction of 3-D buried targets," *IEEE Trans. Geosci. Remote Sens.*, vol. 46, no. 10, pp. 3265–3273, Oct. 2008.
[27] I. Catapano, F. Soldovieri, and L. Crocco, "On the feasibility of the linear sampling method for 3D GPR surveys," *Prog. Electromagn. Res.*, vol. 118, pp. 185–203, 2011.
[28] K. Ren and R. J. Burkholder, "Identification of hidden objects in layered media with shadow projection near-field microwave imaging," *IEEE Geosci. Remote Sens. Lett.*, vol. 15, no. 10, pp. 1590–1594, Oct. 2018.
[29] S. Tantong, B. Camps-Raga, P. Kirawanich, and N. E. Islam, "Near-field microwave imaging techniques for object detection and shape reconstruction," in *Proc. IEEE Region Tech. Conf.*, Fayetteville, AR, USA, Apr. 2007, pp. 299–302.
[30] M. T. Bevacqua and T. Isernia, "Boundary indicator for aspect limited sensing of hidden dielectric objects," *IEEE Geosci. Remote Sens. Lett.*, vol. 15, no. 6, pp. 838–842, Jun. 2018.
[31] M. N. Akıncı, M. Çayören, I. Akduman, and L. Crocco, "A simple approach for estimating the effective electric parameters of 2-D targets," *IEEE Trans. Antennas Propag.*, vol. 66, no. 4, pp. 2026–2034, Apr. 2018.
[32] M. N. Akinci, E. Gose, I. Akduman, and L. Crocco, "Estimation of the effective electrical parameters in two-dimensional transverse electric case," *IEEE Trans. Antennas Propag.*, vol. 68, no. 1, pp. 468–481, Jan. 2020.
[33] R. Potthast, "A study on orthogonality sampling," *Inverse Problems*, vol. 26, no. 7, 2010, Art. no. 074015.
[34] M. N. Akıncı, M. Çayören, and I. Akduman, "Near-field orthogonality sampling method for microwave imaging: Theory and experimental verification," *IEEE Trans. Microw. Theory Techn.*, vol. 64, no. 8, pp. 2489–2501, Aug. 2016.
[35] M. T. Bevacqua, T. Isernia, R. Palmeri, M. N. Akinci, and L. Crocco, "Physical insight unveils new imaging capabilities of orthogonality sampling method," *IEEE Trans. Antennas Propag.*, vol. 68, no. 5, pp. 4014–4021, May 2020.
[36] A. Dell'Aversano, G. Leone, F. Ciaramaglia, and R. Solimene, "A strategy for reconstructing simple shapes from undersampled backscattered data," *IEEE Geosci. Remote Sens. Lett.*, vol. 13, no. 12, pp. 1757–1761, Dec. 2016.
[37] S. Kang and W.-K. Park, "Comparing the imaging performance of MUSIC and linear sampling method," in *Proc. 9th Int. Congr. Image Signal Process., Biomed. Eng. Informat. (CISP-BMEI)*, Oct. 2016, pp. 1298–1301.
[38] A. Brancaccio and G. Leone, "Multimonostatic shape reconstruction of two-dimensional dielectric cylinders by a kirchhoff-based approach," *IEEE Trans. Geosci. Remote Sens.*, vol. 48, no. 8, pp. 3152–3161, Aug. 2010.
[39] S. Dogu and M. N. Akinci, "Assessment of linear sampling method and factorization method for through the wall imaging," in *Proc. 26th Telecommun. Forum (TELFOR)*, Nov. 2018, pp. 18–21.
[40] W. C. Chew, *Waves and Fields in Inhomogeneous Media*. Piscataway, NJ, USA: IEEE Press, 1995.
[41] C. A. Balanis, *Advanced Electromagnetic Engineering*. Hoboken, NJ, USA: Wiley, 1989.
[42] E. D. Caballero, H. Esteban, Á. Belenguer, and V. Boria, "Efficient analysis of substrate integrated waveguide devices using hybrid mode matching between cylindrical and guided modes," *IEEE Trans. Microw. Theory Techn.*, vol. 60, no. 2, pp. 232–243, Feb. 2012.
[43] R. F. Harrington, *Field Computation by Moment Methods*. Hoboken, NJ, USA: Wiley, 1993.
[44] R. Persico, R. Bernini, and F. Soldovieri, "The role of the measurement configuration in inverse scattering from buried objects under the born approximation," *IEEE Trans. Antennas Propag.*, vol. 53, no. 6, pp. 1875–1887, Jun. 2005.
[45] I. Catapano, L. Crocco, R. Persico, M. Pieraccini, and F. Soldovieri, "Linear and nonlinear microwave tomography approaches for subsurface prospecting: Validation on real data," *IEEE Antennas Wireless Propag. Lett.*, vol. 5, pp. 49–53, 2006.

**SOUMYAKANTI MAITI** (Graduate Student Member, IEEE) received the B.Tech. degree in electronics and communication engineering from the West Bengal University of Technology, Kolkata, in 2011, and the M.S. degree in electronics and electrical communication engineering from the Indian Institute of Technology (IIT) Kharagpur, in 2016, where he is currently pursuing the Ph.D. degree with the Advanced Technology Development Center.

**AMITABHA BHATTACHARYA** (Senior Member, IEEE) was born in Kolkata, India, in 1964. He received the B.Tech. (E&ECE) degree from IIT Kharagpur, in 1986, the M.E. (E&TCE) degree from Jadavpur University, in 1994, and the Ph.D. (E&ECE) degree from IIT Kharagpur, in 1998. In 1986, he started his professional career by joining as a Junior Research Engineer in an ISRO sponsored research project at IIT Kharagpur and continued thereafter as a Senior Research Assistant in a DRDO sponsored research project, till 1991. In 1997, he joined SAMEER, Mumbai, and then the Defence Laboratory, Jodhpur, as a Research Scientist. Since 2000, he has been the teaching profession, first as an Assistant Professor with the Electronics and Instrument Department, Indian School of Mines, Dhanbad, in 2007, and the Faculty of Electronics and Electrical Communication Engineering Department, IIT Kharagpur, in 2007. Currently, he is working as a Professor with the Electronics and Electrical Communication Engineering Department and involved in the teaching and research activities with the RF and Microwave Group, E&ECE Department. He has published about 100 research publications in international journals and conferences and has written a textbook on *Digital Communication*. He has been a Principal Investigator of 27 sponsored research projects and consultancies and has conducted 18 sponsored short-term courses around the country, mainly in the areas of electromagnetic environments. He has supervised seven Ph.D. thesis and 38 postgraduate theses. His research interests include microwave imaging, high power microwaves, and microwave stealth technology.

**KAUSHIK DEY** received the B.E. degree in mining, the M.Tech. degree in opencast mining, and the Ph.D. degree in mining. He worked in the field of tunneling and mining sector for few years. He is currently an Assistant Professor with the Department of Mining Engineering, Indian Institute of Technology Kharagpur, India. Prior to joining IIT Kharagpur, he was an Assistant Professor in mining with the National Institute of Technology, Rourkela, and the Indian School of Mines, Dhanbad. He has worked to locate and identify buried objects using GPR in many parts of eastern India. Apart from the same, real-time remote access seismograph, electronic detonator, and remote controlled exploder are also designed by him. He obtained copyrights of three software and one patent. He has published around 70 research papers. His research interest includes application of electronics in rock excavation engineering.